Published in : ChemSusCheml (2025), vol. 18, e20500007
DOI: 10.1002/cssc.202500007
Status : Postprint (Author's version)

NON-ISOCYANATE POLY(HYDROXYURETHANE)-BASED NETWORKS AS SOLID POLYMER ELECTROLYTES FOR LITHIUM METAL BATTERIES

Ashish Raj

Institute of Condensed Matter and Nanoscience (IMCN), Université catholique de Louvain, Louvain-la-Neuve, Belgium.

Bruno Grignard

Center for Education and Research on Macromolecules (CERM), CESAM Research Unit, University of Liège, Liège, Belgium – Federation of Researcher in Innovation Technologies for CO2 transformation (FRITCO2T research platform), University of Liège, Liège, Belgium.

Christophe Detrembleur

Center for Education and Research on Macromolecules (CERM), CESAM Research Unit, University of Liège, Liège, Belgium – WEL Research Institute, Wavre, Belgium.

Jean-François Gohy

Institute of Condensed Matter and Nanoscience (IMCN), Université catholique de Louvain, Louvain-la-Neuve, Belgium.

Abstract. We report here on the facile synthesis of poly(hydroxyurethane) (PHU) networks obtained via the ring-opening of cyclic carbonates present on bio-based carbonated soybean oil by poly(ethylene glycol) (PEG) segments of various lengths and functionalized at both ends by amines. We also explore the possibility to prepare PHU-poly(epoxy) mixed networks by additionally incorporating PEG segments functionalized at both ends by epoxides in the reaction mixture. The accordingly obtained polymer networks possess high flexibility and a good interfacial stability. After salt loading, the solid polymer electrolyte (SPE) membranes based on PHU and PHU-poly(epoxy) mixed networks exhibit ionic conductivities in the range of ~$10^{-4.5}$ to 10^{-5} Scm^{-1} at 60°C with oxidation stability > 4.2 V versus Li/Li^{+}. Further, their long-term compatibility with lithium metal has been investigated for more than a hundred cycles in stripping and plating experiments. Those results drive the PHUbased networks toward the development of electrolytes with a high degree of control on structure and properties, dealing with the trade-off of mechanical and electrochemical properties usually met with PEG-based SPEs.

Keywords. Bio-based, Solid-state battery, Polymer electrolytes, LiTFSI, Lithium anode.

Published in : ChemSusChemI (2025), vol. 18, e20500007
DOI: 10.1002/cssc.202500007
Status : Postprint (Author's version)

Introduction

Lithium-ion batteries have already made their place in the market for more than two decades.[1] However, they are required to outperform their energy density with improved safety and processing. These aspirations can only be achieved with high-energy-density electrodes and safer electrolytes, specifically solid-state electrolytes (SSEs). High voltage cathodes development has been progressive throughout the timeline of lithium-ion batteries research with periodic challenges for anodes either with compatibility or stability with electrolytes. Among those, silicon-based materials and lithium metal anodes possess the highest theoretical capacity, with the later showing as much as 3860 $mAhg^{-1}$.[2] However, they do not sound very safe with the current technology based on flammable liquid electrolytes.[3] Therefore, replacing liquid electrolytes with solid ones would not only remove the drawbacks of flammability, leakage, and short-circuit due to dendrite growth and packaging, but also provide lithium metal compatibility and a broad voltage window for high-voltage cathodes application as well. In addition, this replacement brings to other remarkable advantages aligning with both electrochemical and mechanical properties. SSE electrolytes are supposed to offer broad oxidation stability (beneficial for high voltage cathodes without electrolyte decomposition), lightweight, flexibility, easy stack, robustness, safety (non-flammable), and thus costeffectiveness.[2, 4] On the contrary, SSEs offer low ionic conductivity and poor interfacial compatibility. So far, inorganic solid electrolytes have outperformed solid polymer electrolytes (SPEs), but the latter excites with good mechanical properties and processability.

Over the years, various classes of polymers have been tested with varying architecture, topology, and molecular weight in their pristine or copolymer state. The availability of polar groups for lithium ion complexation via weak coordination is always desired in any polymer as a conduction host. Some of the wellknown polymers explored so far in batteries include PEG,[5–6] polycarbonates,[7–8] polyvinylidene fluoride (PVDF),[9–10] poly(methyl methacrylate),[11–12] polysiloxanes,[13–14] polyurethanes,[15–17] *etc.* While most of those exhibited potential performance in their investigation, they underperform on other required parameters, such as salt solvation or oxidation stability, which demands more polymer engineering.[18–22] In concern to addressing those trade-offs in one polymer, a variety of synthetic methods and techniques found their way like block copolymers, blends, plasticization, hybrid polymers with inorganic fillers, *etc.*[18–22] Higher salt dissociation and mobile charge carriers contribute to higher ionic conductivity and higher transference number. The ability to prevent dendrite growth and form a stable solid electrolyte interphase (SEI) with decent compatibility mark crucial indicators for a good electrolyte.[23–25]

Poly(hydroxyurethane)s (PHUs), like the parent polyurethanes (PUs), combine soft and hard segments in one polymer. PUs, first discovered by Otto and co-workers,[26] are being used in many industrial products, including coatings, paints, adhesives, and resins. However, the first report on PUs as SPEs in 1980 highlighted their potential in batteries.[27] The conductivity was speculated to be facilitated by soft segments and mechanical properties via hard segments within the same polymer.[16] In later reports, isocyanate-based PUs have been exploited in various forms involving copolymers, blends, hybrids, showing conductivities◦ as low as ~10^{-8} to as high as ~10^{-5} Scm^{-1} at 25°C.[28–29] Some reports have focused on natural oil-based monomers-derived PUs, exhibiting decent Li-ion conduction,

Published in : ChemSusCheml (2025), vol. 18, e20500007
DOI: 10.1002/cssc.202500007
Status : Postprint (Author's version)

such as jatropha,[30] palm kernel oil,[31] castor oil.[32] Moreover, when compared to non-crosslinked materials, SPE networks were reported to provide better mechanical as well as electrochemical properties on the potential addition of additives, fillers, plasticizers, *etc.* Scardi *et al.* demonstrated that SPEs obtained by reacting palm kernel oil polyol and 2,4methylene diphenyl diisocyanate could reach a conductivity of 7.6×10^{-4} Scm^{-1} at RT after plasticization with ethylene carbonate.[31]

While PUs are often synthesized via reaction between diisocyanates and alcohol/polyol in the presence of a catalyst, PHUs are presented as non-isocyanate polyurethanes (NIPUs). They are prepared using different techniques, among them the aminolysis of cyclic carbonates.[33–34] Cyclic carbonates and derived PHUs are gaining more interest due to their highly sustainable synthetic pathway via coupling of CO_2.[8, 35] Moreover, the introduction of dynamic covalent bonds in PHUs-based electrolytes is able to confer interfacial self-healing behaviour to the system.[36] Supramolecular interactions and dynamic covalent bonds have been widely investigated in batteries because of their self-healing abilities. Electrochemical reactions in batteries normally lead to structural changes, which can cause mechanical damage and degradation of polymers applied to electrodes or electrolytes, and ultimately cause the batteries to be non-functional over the repeated cycling process. The relatively high volumetric changes of the Li metal anode result in straining or even cracking of the protective SEI layer, which accelerates the inhomogeneous Li deposition and leads to rapid growth of Li dendrites in the microcracks. If those microcracks can be fully restored in time, lithium-based batteries will keep working steadily. For example, an artificial SEI layer with intrinsic self-healing functions can timely restore the surface pinholes or cracks caused by the puncture of Li dendrites, giving the Li metal anode with stable cycling performance.[37]

Here, we report a series of SPEs based on PHU, synthesized via catalyst-free addition reaction between carbonated soybean oil (CSBO) bearing on average 6 carbonates and PEG segments of various lengths terminated at both ends by amines (see Scheme 1) to tune the mechanical and electrochemical properties. The network results from the ring-opening reaction of the cyclic carbonate (CC) rings of CSBO by the nucleophilic amines (Scheme 1). Since CC rings show good lithium solvation and are widely used in the side chains and main chain of SPEs for their better transport properties,[7, 38] the stoichiometric ratio between CC rings from CSBO and amino groups from PEG segments is varied to leave some CC rings unopened in the final networks in order to study the impact on the ionic conductivity in the final SPE. Furthermore, with the aim to produce self-standing membranes for further use as SPEs in solid-state batteries, we introduce short and long PEG segments together while forming the PHU network to obtain the best compromise between crosslinking density required for mechanical properties and the presence of long flexible PEG segments needed for ionic conductivity. Additionally, we explore the possibility of building up a mixed network by introducing another ring-opening reaction by adding poly(ethylene glycol) diglycidyl ether (PEGDCE) in the reaction mixture (Scheme 2). The lithium metal compatibility with our SPE membrane is finally demonstrated by cycling and postmortem XPS analysis.

Published in : ChemSusCheml (2025), vol. 18, e20500007
DOI: 10.1002/cssc.202500007
Status : Postprint (Author's version)

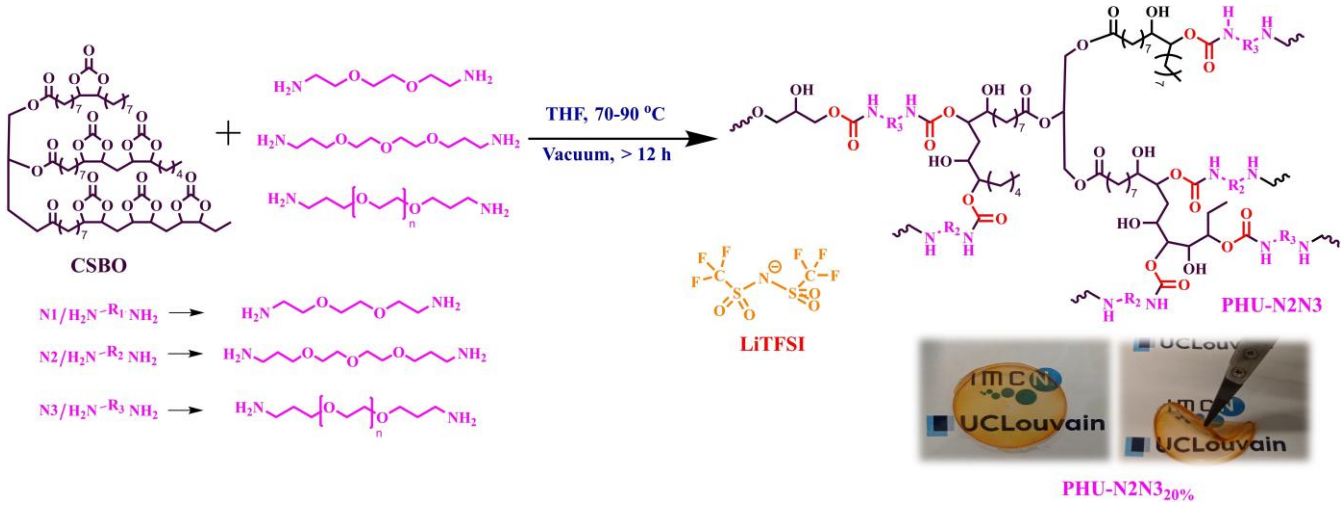

Scheme 1. Synthesis of poly(hydroxyurethane) analogues with possible network structure, (bottom-right). PHU networks are obtained by reaction between CSBO and various α,ω-diamino PEG (denoted as N1, N2, and N3). Pictures of PHU@N2N3 (75 mol% of N2 and 25 mol% of N3) films with 20 wt% LiTFSI as labelled in subscript.

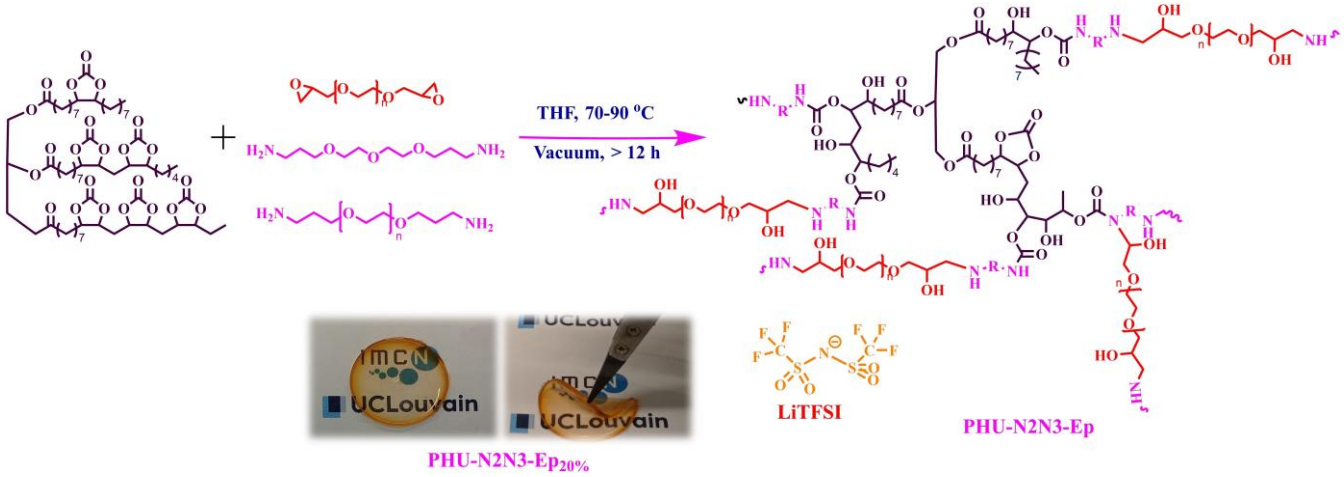

Scheme 2. Synthesis of idealized mixed poly(hydroxyurethane)-poly(epoxy) (PHU@Ep) networks with PEGDCE (bottom-right: picture of PHU–N2N3-Ep films (75 mol% of N2, 25 mol% of N3, and 100 wt% of PEGDCE with respect to CBSO)), subscript indicates x-wt% LiTFSI).

Results and Discussion

SYNTHESIS OF NETWORKS

In this contribution, PHU networks and PHU-poly(epoxy) (PHU–Ep) mixed networks were synthesized via an isocyanate and catalyst-free, sustainable synthetic approach at mild temperature and reaction conditions. The synthesis of the polymer networks is depicted in Schemes 1 and 2 for PHU and mixed PHU–Ep, respectively. The reaction between CC and diamine follows a ring opening mechanism with

Published in : ChemSusChemI (2025), vol. 18, e20500007
DOI: 10.1002/cssc.202500007
Status : Postprint (Author's version)

intermediate steps as highlighted elsewhere.[39] At first, we studied the reaction between CSBO and a bis(3-aminopropyl)-terminated poly(ethylene glycol), PEGTA (denoted as N3) containing ~32 ethylene oxide units. The molar ratio between CC groups in CSBO and the N3 diamine was varied in presence of 15 wt% of LiTFSI. The reaction was monitored using Fourier-transform infra-red spectroscopy (FTIR) by following the increase in the intensity of urethanes bands (Figure S1). A CSBO:N3 1:3 molar ratio corresponds to the assumption that all six rings of CSBO are opened. Similarly, the CSBO:N3 2:5 molar ratio targets the opening of 5 CCs rings and so on for other analogues. As it can be observed in Figure S1, the formation of PHU network was confirmed by the appearance of a characteristic band at ~1716 cm^{-1}(C=O urethane) along with a band at ~1738 cm^{-1} ("ester" part of the urethane group), while the characteristic band of the remaining CC group appears at around ~1799 cm^{-1}. It should be noted that CC groups are still detected (although giving a weak signal) for the CSBO:N3 1:3 molar ratio for which complete ring opening was expected in case of a quantitative reaction. This could be explained by the unequal accessibility of all carbonate rings and relatively short reaction time. However, CSBO:diamine 1:3 molar ratio will be only considered for the next experiments since we noted that a higher amount of unopened CC is resulting in a lower crosslinking density for the accordingly obtained PHU network and, hence, in poor mechanical properties for the final SPE membrane. Unfortunately, none of the PHU–N3 network (whatever the CSBO/N3 stoichiometry or the added amount of LITFSI) was giving rise to a self-standing membrane suitable for further investigation in batteries.

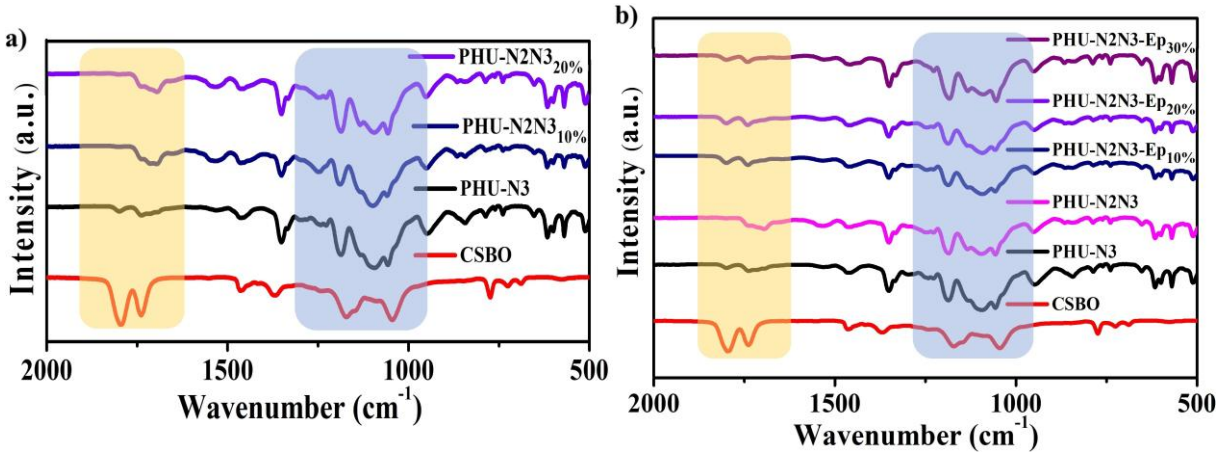

Figure 1. FTIR spectra of PHU and PHU–Ep with varying formulation, a) PHU–N2N3$_x$; and b) PHU–N2N3-Ep$_x$ in comparison to PHU–N3 and CSBO, respectively (where, 75 mol% of N2, 25 mol% of N3, 100 wt% of PEGDE with respect to CBSO and x wt% of LiTFSI).

In order to get membranes with better mechanical properties, our first strategy was to increase the yield of the crosslinking reaction leading to the PHU network. This could be achieved by mixing N3 with shorter diamines during PHU preparation, since the latter are believed to show higher accessibility to CC rings. Following this idea, PHU-NXNY networks have been accordingly synthesized by mixing N3 with two other short α,ω-diamino molecules which differ from their number of ethylene oxide (EO) units, i.e. 2 in 2,2'-(ethylenedioxy)bis(ethylamine), EDEA (denoted as N1) and 3 in 4,7,10-trioxa-1,13-

Published in : ChemSusChemI (2025), vol. 18, e20500007
DOI: 10.1002/cssc.202500007
Status : Postprint (Author's version)

tridecanediamine, TDD (denoted as N2). For all experiments, the CSBO:diamines molar ratio was adjusted 1:3 to maximize the number of opened CC rings. The best compromise was obtained with a combination of 75 mol% of N2 and 25 mol% N3, as shown in the picture of the resulting SPE membrane in Scheme 1. In the following, only this composition will be considered for further investigation. The high number of EO units sourced from N3 is crucial for Li^+ conduction while N2 increases the yield of ring-opening reaction due to its higher accessibility to CC rings.

In further attempts, another strategy was designed to target better Li^+ ions transport properties without losing the freestanding nature of the SPE resulting from network formation (Scheme 2). This strategy consists in using an additional crosslinking reaction beside the ring-opening of CCs by nucleophilic amines. Indeed, we have shown that the ring-opening reaction of CCs by amines is not complete, probably because of a restricted access to the CC groups of CSBO due to steric constraints. Because amino groups are added in a stoichiometric ratio to CCs, this means that free amino groups are still available once the reaction towards the PHU network is ended. Those unreacted amino groups could therefore react with another, less sterically hindered reactive group. More precisely, we introduced PEG chains bearing epoxides at both ends (PEGDCE), that are expected to react with left unreacted amino groups from N2 and N3 following a similar strategy for PHU foams, leading to hybrid PHU.[39] An idealized representation of this hypothesized sequential reaction is depicted in Scheme 2 and should lead to a mechanically reinforced network due to a better crosslinking density. Practically, PEGDCE has been mixed with CSBO and the different α,ω-diamino-functionalized PEG to obtain PHU-NXNY–Ep mixed networks. The optimized ratio and reaction conditions for PHU–N2N3-Ep were translated from PHU–N2N3 without change. Since it is very difficult to estimate the amount of unreacted amino groups available for reaction with PEGDCE, the identical weight amounts of CSBO and PEGDE have been introduced in the mixture. Moreover, the PEGDCE epoxy monomer contains ~8 EO units, which is beneficial for ionic conduction.

The mechanical properties of both SPEs (PHU–N2N3 and PHU–N2N3-Ep with 20 wt% LiTFSI) were assessed using rotational rheology (Figure S2). The comparison of G' value in the linear viscoelastic region (LVR) during the strain-sweep test (angular frequency=10/s, strain between 0.01% and 100%) revealed a threefold increase in G' for the membrane containing epoxide (Figure S2b) in comparison to epoxide free membrane (Figure S2a) confirming the improvement of the mechanical properties. Frequency sweep experiment conducted in the LVR (strain=0.1%) confirms the cross-linked nature of both SPE with a G'>G'' and Tan δ<1 on the entire range of tested frequency (Figures S2c and S2d). Interestingly, the reduced ratio between G' and G''=10 at low frequency suggests that the proportion of mobile polymer segments (not fully cross-linked) is not negligeable, so still conferring chain mobility and energy dissipation within the SPE containing epoxy.

FOURIER TRANSFORM INFRA-RED SPECTROSCOPY

In order to get further insight into the crosslinking reactions, Fourier transform infra-red spectroscopy (FTIR) was systematically employed to characterize the accordingly obtained PHU networks, as shown in Figure 1. In PHU–N3, the carbonyl peak corresponding to CC at 1796 cm^{-1} was retained with a slight shift at 1801 cm^{-1} and with lower intensity as observed in Figure 1a. As discussed before, this hints at

Published in : ChemSusCheml (2025), vol. 18, e20500007
DOI: 10.1002/cssc.202500007
Status : Postprint (Author's version)

the incomplete CC ring opening either due to a low concentration of crosslinkers or inaccessible CC rings.

However, the CC carbonyl peak is still visible in the case of PHU–N2N3 with the appearance of a urethane bond signal at 1701–1696 cm^{-1} and 1713–1716 cm^{-1}. The CC ring-opening reaction is obviously not complete in this case too.

The ester signal (–RCOOR–) from CSBO at 1739 cm^{-1} was detected at 1740 cm^{-1} for PHU–N3 and slightly shifted to 1738 cm^{-1} and 1736 cm^{-1} for PHU–N2N3$_{20\%}$ and PHU–N2N3$_{10\%}$, respectively. Other characteristic signals involved –OH stretching at 3451 cm^{-1}, 3380 cm^{-1}, and 3390 cm^{-1}, while -NH- signal at 1531 cm^{-1}, 1537 cm^{-1}, 1533 cm^{-1} for PHU–N3, PHU–N2N3$_{10\%}$, and PHU–N2N3$_{20\%}$, respectively (Figure S3). A strong aliphatic ether (–C–O) signal was recorded around 1106 cm^{-1} along with C–N stretching in the range of 1250 cm^{-1}–1275 cm^{-1} in corresponding PHU networks.

Similarly, referring to Figures 1b for PHU–N2N3-Ep, incomplete ring opening of CC was observed by comparing spectra of PHU–N2N3-Ep with PHU–N3 and PHU–N2N3. The CC carbonyl (–C=O) peak was marked within 1798–1800 cm^{-1} in addition to the ester (–RCOOR) around 1738–1741 cm^{-1}. Conversely urethane stretching was recorded with higher broadening due to lesser carbamate formation and higher salt concentration in a similar region as of PHU–N2N3. However, there was no strong signal detected from epoxy besides a slightly weak and broadened peak around 880 cm^{-1} specifically for PHU–N2N3-Ep$_{10\%}$ and PHU–N2N3-Ep$_{20\%}$. This points towards the reaction of all epoxy groups of PEGDCE with the unreacted amines of N2 and N3. This also indicates that the estimation about the added amount of PEGDCE was suitable. The good solvation of LiTFSI was validated from signals in the range around 900–700 cm^{-1} corresponding to S–N stretching from $TFSI^-$ ions and C–O stretching around 900 cm^{-1}.

THERMAL PROPERTIES

Thermal analysis was performed using differential scanning calorimetry (DSC) and thermogravimetric analysis (TGA) with parameters as mentioned in the experimental section. The polymer melting (T_m), crystallization (T_c), and glass transition (T_g) temperatures were monitored via DSC in the -70°C to 100°C range. Among all precursors, only N3 possesses a solid nature at room temperature, while N1 and N2 are liquids, and PEGDCE and CBSO are viscous fluids. CSBO shows a low T_g, which increases with salt concentration with no crystallization, [8] whereas T_m and T_c were recorded at 50.1°C and 20.1°C, respectively, for N2 (Figures 2a and 2b). A cold crystallization phenomenon was observed in PHUs without LiTFSI with T_g at -48.8°C. However, LiTFSI loaded PHU–N2N3 networks showed only amorphous behaviour with higher T_g of -43.7°C, -44.2°C, and -40.8°C respectively for 10, 15, and 20 wt% of added LiTFSI. This trend in T_g is predicted to be non-conclusive due to low differences in salt concentration. The PHU–N2N3-Ep network with 100 wt% of PEGDCE to CSBO was also subjected to DSC measurements. The network without LiTFSI showed a lower T_g of -43.9°C relative to PHU–N2N3, while a similar decrement was also observed with LiTFSI, to -37°C, -37.8°C, and -33.5°C for PHU–N2N3-Ep$_{10\%}$, PHU–N2N3-Ep$_{20\%}$, and PHU–N2N3-Ep$_{30\%}$, respectively, as indicated in Figure 2b.

Published in : ChemSusCheml (2025), vol. 18, e20500007
DOI: 10.1002/cssc.202500007
Status : Postprint (Author's version)

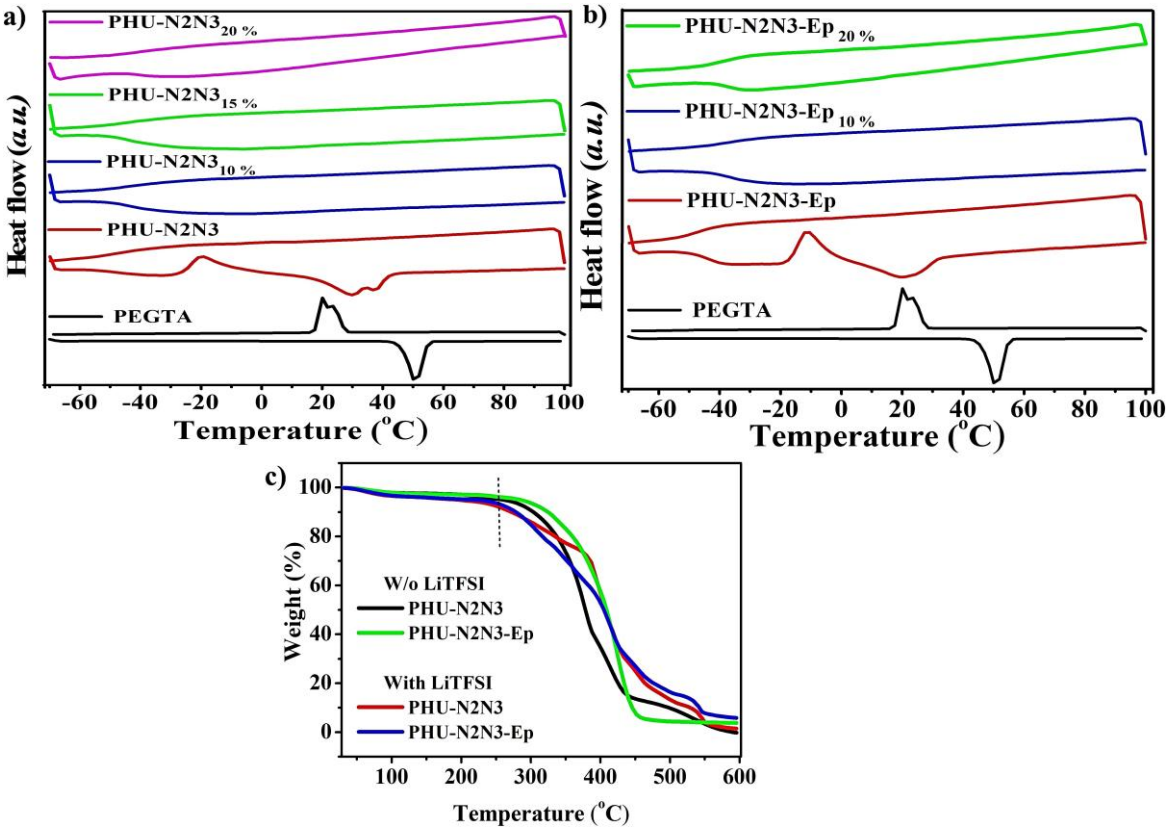

Figure 2. DSC thermograms of PHU analogues, a) PHU–N2N3 and b) PHU–N2N3-Ep in comparison to PEGTA (N3); c) Thermogravimetric analysis of PHU–N2N3 and PHU–N2N3-Ep with and without 20 wt% LiTFSI (75 mol% of N2, 25 mol% of N3, 100 wt% of PEGDCE with respect to CBSO).

Thermal degradation of the networks was analyzed by TGA measurements in N_2 supply in the temperature range of 30°C to 600°C for a comparative analysis of PHU analogues with and without LITFSI (Figure 2c). The analysis can be split into multiple components as depicted from the derivative of TGA. In the beginning, the slight weight % loss could be correlated◦ to adsorbed moisture for all the samples until 100°C. Major decomposition◦ for almost all the analogues starts nearly ~250°C and with polymer without LiTFSI at slightly higher T_d. Among PHU–N2N3 and PHU–N2N3-Ep, higher thermal stability temperatures, >500°C. LiTFSI decomposition was observed at is observed for plasticized networks as evident at higher around 500°C.

IONIC CONDUCTIVITY

Coin/Swagelok cells with PHU networks SPEs membranes were subjected to potentiostatic electrical impedance spectroscopy (PEIS) for conductivity measurement at various temperatures in symmetric blocking cells with stainless steel electrodes. Nyquist plots with real and imaginary impedance were recorded and analyzed for electrolyte◦ resistance (as depicted in Figures S4a and S4b at 30°C). The conductivity (σ) was calculated using equation 1, which depends on parameters such as length and area of the film besides resistance,

Published in : ChemSusCheml (2025), vol. 18, e20500007
DOI: 10.1002/cssc.202500007
Status : Postprint (Author's version)

$$\sigma = \frac{l}{R_b S} \quad (1)$$

where R_b is bulk electrolyte Ohmic resistance from AC impedance, l and S are thickness and the surface area of polymer electrolyte, respectively.

Equation 2 was used for modelling conductivity with VogelFulcher-Tamman (VFT) behaviour,

$$\sigma T^{1/2} = Ae^{-\frac{E_a}{K_b}(T-T_0)} \quad (2)$$

where A is the conductivity pre-exponential factor, T is the absolute temperature, T_0 is the Vogel scaling temperature at which the free volume disappears or at which free entropy becomes zero following approximation as $T_0 = (T_g - 50\ K)$, E_a is the pseudo-activation energy of ion transport, and k_b is Boltzmann constant.[40–41]

The conductivity of PHU–N2N3 was compared with various added amount of LITFSI (10–20 wt%) from 0–80°C and was depicted in a logarithmic conductivity plot with temperature following Arrhenius model (Figure 3a). PHU–N2N3 exhibited best conductivity of $1.6x10^{-4}$ Scm^{-1} at 80°C for 20 wt% added LITFSI. At 20°C, higher conductivity was recorded for PHU–N2N3$_{15\%}$, i.e. 4.07×10^{-6} Scm^{-1}. The trend of conductivity versus temperature with certain anomalies could be related to free ion pairs coupled with restricted ion mobility due to crosslinking. While using the VFT model of conductivity, we deduced the higher conductivity trend in PHU–N2N3$_{10\%}$ at lower temperatures and PHU–N2N3$_{20\%}$ at higher temperatures, as shown in Figure 3b.

The conductivity of PHU–N2N3-Ep bearing cyclic carbonate rings was measured with LiTFSI concentration (10–30 wt%), as indicated in Figure 3c. A conductivity of 3.9×10^{-6} Scm^{-1} at 20°C was observed for PHU–N2N3-Ep$_{20\%}$. The highest conductivity was obtained at 80°C to be $1.2x10^{-4}$ Scm^{-1} for PHU–N2N3-Ep$_{20\%}$. For the same salt concentration, PHU–N2N3-Ep$_{20\%}$ exhibited better ionic conductivity than PHU–N2N3$_{20\%}$ until 50°C and slightly lower conductivity from 60°C onwards. While aligning the conductivity with VFT model for PHU–Ep mixed networks, we did not find much difference as shown in Figure 3d. We could speculate the higher crosslinking nodes and an increased rigidity in the PHU–N2N3-Ep$_{20\%}$ network, lowering segmental motion. However, it is not clear at this stage if the unreacted CC exerts a positive effect on the overall ionic conductivity. We speculate to understand the effect of CC with precise quantification of opened rings. For further electrochemical measurements, PHU–N2N3-Ep$_{20\%}$ was explored owing to the good compromise in the conductivity of 4.49×10^{-5} Scm^{-1} (at 60°C), number of charges carrier, and mechanical properties. Finally, it should be highlighted than PHU analogues demonstrated higher conductivity than CSBO, as shown in Figure S5.

Published in : ChemSusCheml (2025), vol. 18, e20500007
DOI: 10.1002/cssc.202500007
Status : Postprint (Author's version)

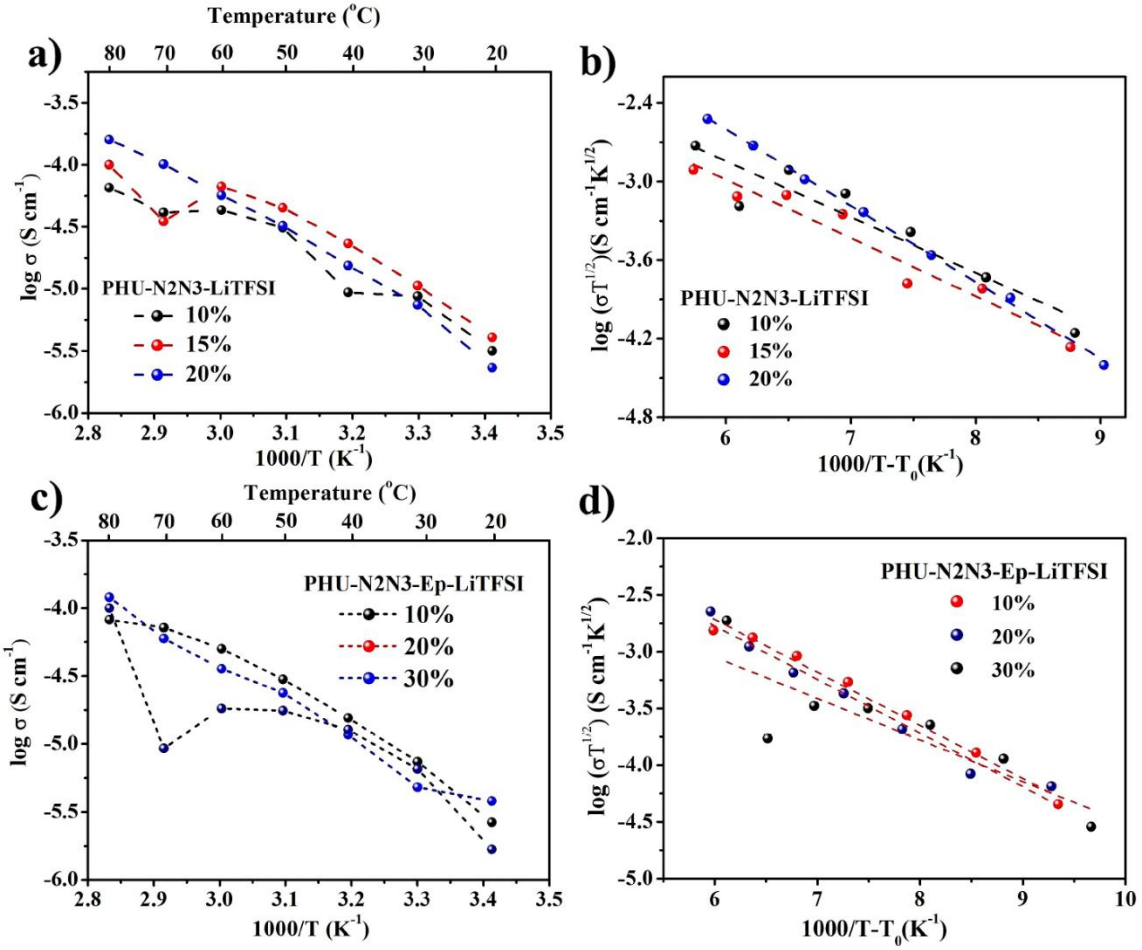

Figure 3. Temperature dependent ionic conductivity for investigated SPE networks; a) and c) Arrhenius model, b) and d) VFT model, a) and b) PHU–N2N3-LiTFSI (10-20 wt%); c) and d) PHU–N2N3-Ep-LiTFSI (10-30 wt%), respectively (75 mol% of N2, 25 mol% of N3, 100 wt% of PEGDCE with respect to CBSO).

ELECTROCHEMICAL STABILITY WINDOW

Oxidation potential limitation for an electrolyte is investigated to find the threshold voltage at which it can channelize ions without decomposition. A wide electrochemical stability window (ESW) at higher voltage allows the higher voltage cathodes to store more reversible energy. ESW, as measured using linear scanning voltammetry (LSV), is presented in Figure 4 and Figure S6. At the scan rate of 0.5 mVs^{-1}, the oxidation stability limit of $PHU–N2N3_{20\%}$ was observed to be around E_{ESW} >4.01 V vs Li/Li+ with stainless steel cathode. The latter was recorded to be higher in the case of $PHU–N2N3\text{-}Ep_{20\%}$ (subscript indicates 20 wt% of LiTFSI for both PHU analogues), i.e. E_{ESW} >4.24 V vs Li/Li^+ in similar conditions and parameters.

Published in : ChemSusCheml (2025), vol. 18, e20500007
DOI: 10.1002/cssc.202500007
Status : Postprint (Author's version)

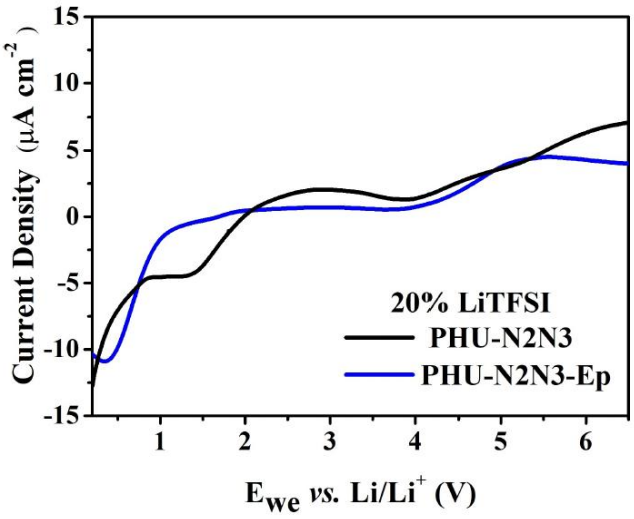

Figure 4. Linear sweep voltammetry analysis of PHU-based-SPEs with 20 wt % LiTFSI.

STRIPPING AND PLATING

The electrolyte/lithium metal compatibility has been tested via lithium stripping and plating under time-dependent constant current cycling, as represented in Figure 5a. The voltage-time plot for PHU–$N2N3_{20\%}$ qualitatively explains electrolytic decomposition with lithium metal. Owing to the conductivity of the electrolyte, lower current density has been employed in the range of 0.52 μAcm^{-2} to 4.55 μAcm^{-2} with the cut-off voltage of +2 V to -2 V. The first 2^{nd}-3^{rd} cycles offered huge kinetic hindrance to lithium transport leading to high overpotential to cutoff voltage at 1.3 μAcm^{-2}. Subsequently, a lower current density of 0.52 μAcm^{-2} was applied for almost 100 cycles, which recorded a clear decreasing overpotential, i.e. 0.22 V in stripping and -0.3441 V while plating at the 50^{th} cycle. As a result of interfacial stabilization, a reduction in the interfacial resistance could be observed. Furthermore, the overpotential increased drastically when the current density was increased by 4 times, resulting in a stripping voltage of 0.16 V at the 320^{th} cycle. However, despite doubling the current density to 4.55 μAcm^{-2}, we did not observe much drastic increment in the voltage.

The overpotential stabilized from 642 h (321^{st} cycles) onward and recorded over constant values until measured cycles for 1042 h (521 cycles) with stripping-plating of 0.37 V and -0.32 V, respectively. The stable SEI even after a long number of cycles was evident from constant overpotential recorded from 321^{st} cycles onward.

Published in : ChemSusCheml (2025), vol. 18, e20500007
DOI: 10.1002/cssc.202500007
Status : Postprint (Author's version)

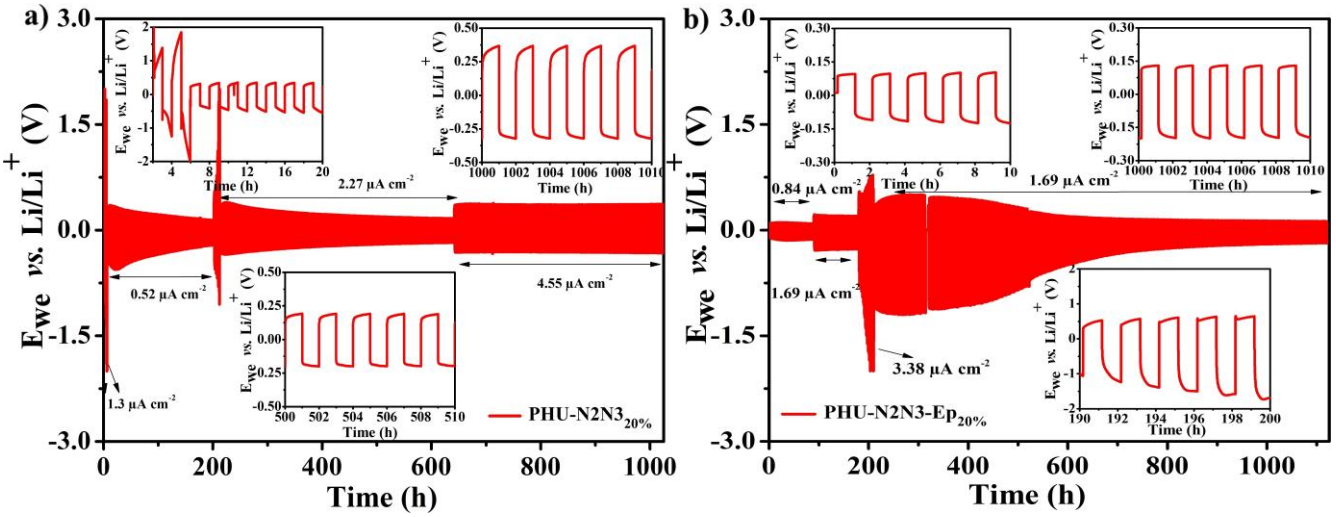

Figure 5. Galvanostatic charge-discharge voltage profile for stripping-plating at various current densities at 60°C with Li |PHU-SPEs |Li symmetric cells, a) PHU–N2N3 and b) PHU–N2N3-Ep, respectively (insets: magnified plots at respective time demonstrating the constant over potential).

As far as stripping and plating in PHU–N2N3-Ep$_{20\%}$ are concerned, higher overpotential was expected in those cells due to relatively lower ionic conductivity. As a result of initial cycling at the current density of 0.84 μAcm^{-2}, the overpotential was ~0.1 V. While for subsequent 45 cycles, an almost constant overpotential of ~0.22 V was recorded on the doubling of the current density. However, an abrupt increment to 3.38 μAcm^{-2} led to higher polarization of ~0.7 V and -2 V during charge and discharge, respectively. For remaining long-term cycling, 1.69 μAcm^{-2} was chosen and cycled for more than 400 cycles with constant decreasing overpotential and stabilization from the 400th cycle onwards at nearly ~0.15 V. Inset in the Figure 5b shows the voltage profile during the last cycles of the stripping-plating, averaging at ~0.15 V. This supports the efficient transport of lithium ions within the electrolyte and SEI at certain current density. Larger polarization at a relatively higher current explains lower conductivity and parasitic electrolytic decomposition.

POST-MORTEM ANALYSIS OF CYCLED CELLS

XPS analysis on the Li anode and SPE surfaces for lithium symmetric cells was performed to probe their interfacial composition after stripping and plating for more than 1000 h. The C1s peak at 284.8 eV was used as a reference to calibrate the binding energy. The survey spectra detected the desired elements like C, O, Li, F, N and S originating from the SEI layer or decomposition reactions are shown in Figure 6 for SPE membranes of PHU–N2N3 and PHU–N2N3-Ep (refer to Figure S7 for abundance % bar chart plot). The C1s spectra in both SPEs excluding the adventitious carbon can be attributed to C–C/C–H, C–O/N, O–C–O/C=O, and O–C=O/CO_3^{2-} (inorganic carbonates) with the binding energy of ~284.9 eV, 286.3 eV, 287.9 eV, and 288.8 eV for PHU–N2N3 and at ~284.8 eV, 286.2 eV, 287.9 eV, and 288.8 for PHU–N2N3-Ep, respectively, as shown in Figures 7a and 7d. Referring to the simulation performed in our previous report, C=O formation from carbamate cleavage is anticipated.[24]

Published in : ChemSusCheml (2025), vol. 18, e20500007
DOI: 10.1002/cssc.202500007
Status : Postprint (Author's version)

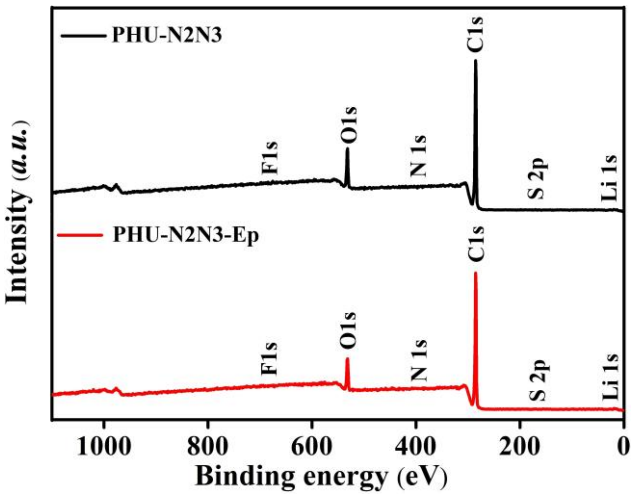

Figure 6. Survey spectra of surface of cycled PHU based SPEs from Li-Li cells after 500+ cycles of stripping and plating.

SEI stabilized by LiF formation was detected at 688.2 eV (0.2%) and 688.3 eV (0.2%), while -CF_3 corresponding to LiTFSI at 688.2 eV (1.2%) and 688.3 eV (0.3%) in respective PHUs (Figures 7b and 7d). From the higher proportion of LiF formation for the SPE membranes of PHU–N2N3-Ep, it can be deduced that the addition of epoxy and ether groups increased the reactivity with lithium and thus higher decomposition compared to PHU–N2N3.[24] A similar finding has been witnessed when the HR-XPS of S2p for both SPE membranes are compared in Figures 7c and 7f. A sharper signal for SO_x was observed in PHU–N2N3-Ep than in PHU–N2N3. The quantification table can be found as supporting information (Figure S8) along with HR-XPS of other elements, such as O1s, N1s, and Li1s. These surface analyses backed the decent stripping and plating experiments over hundreds of cycles due to stable electrolyte decomposition and SEI formation. The quantification table for the elements can be referred from Table S1.

Published in : ChemSusCheml (2025), vol. 18, e20500007
DOI: 10.1002/cssc.202500007
Status : Postprint (Author's version)

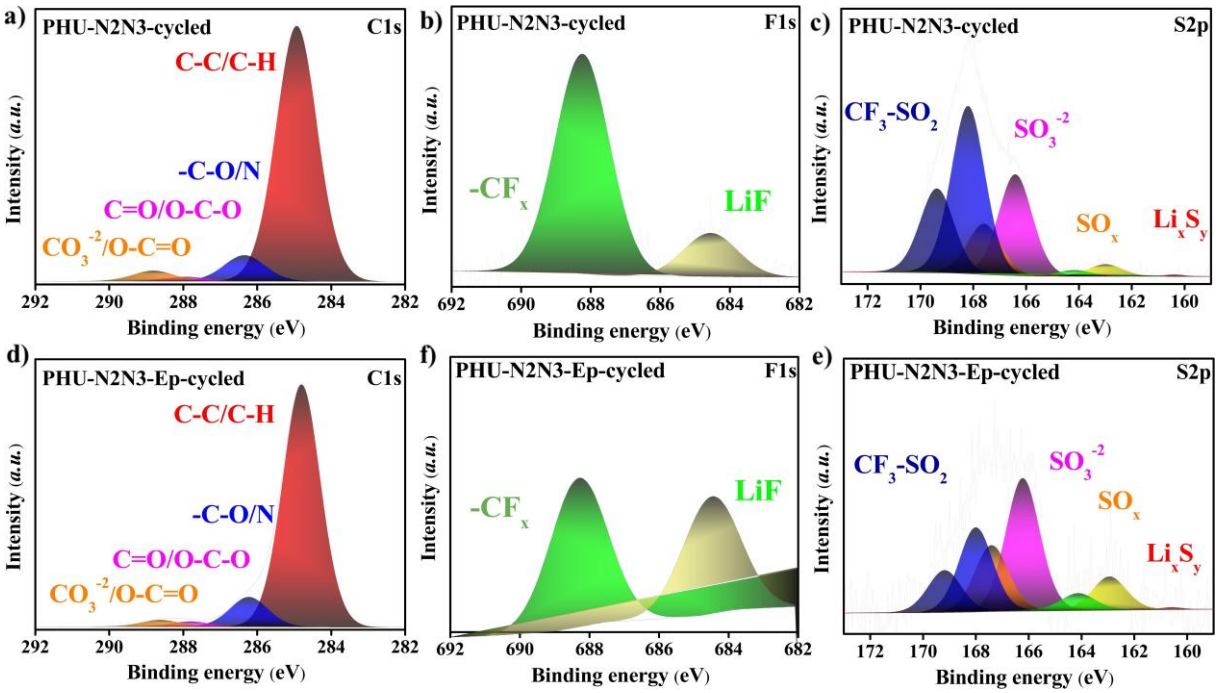

Figure 7. HR-XPS of a) and c) carbon, b) and d) fluorine and e) sulphur at the surface of cycled PHU-based SPE films after stripping and plating with Li-Li cells.

LI-METAL BATTERY PROTOTYPES

Solid-state battery prototypes using the most promising PHU–N2N3-$Ep_{20\%}$ SPE with Li metal anodes and LFP cathodes were tested by galvanostatic cycling with potential limitation (GCPL) technique over the voltage of 2–4 V (Figure 8). Those cells exhibited a discharge capacity of 114.96 $mAhg_{@1}$ at a Crate of 0.1 C at 60 C with the polarization of almost ~0.179 V in the 1st cycle as in Figure 8a. The polarization drops in the subsequent cycles to ~0.084 V and ~0.0341 V in the 10th cycles and 30th cycle, respectively. This could be credited to the stabilized interface due to the beneficial decomposition of SPE at the lithium surface. However, the discharge capacity drop is also observed to 108.79 $mAhg^{-1}$ and 94.63 $mAhg^{-1}$ at the respective 10th and 30th cycle. The capacity-cycle plot shows the fading capacity with increasing Coulombic efficiency (up to ~97.8%) as demonstrated in Figure 8b. The fading could be also an indication of high diffusion barriers between the electrodes and electrolyte. Nevertheless, this preliminary cycling test on PHU–N2N3-$Ep_{20\%}$ showed the potential performance of our SPEs.

Conclusions

More and more emphasis needs to be placed on sustainable precursors and approaches for polymer electrolytes given the high concern for the impact of chemicals on clean energy. We have attempted here to address the issue of the environmental footprint by utilizing a bio-based precursor for the synthesis of lithium salt loaded PHU analogues as potential solid-state electrolytes from lithium-ion

Published in : ChemSusCheml (2025), vol. 18, e20500007
DOI: 10.1002/cssc.202500007
Status : Postprint (Author's version)

conduction. The accordingly obtained self-standing electrolyte membranes demonstrated good flexibility and interfacial contact, as speculated from low T_g around -40°C. The ionic conductivity of the PHU–N2N3 and PHU–N2N3-Ep samples remains in the order of 10^{-5} Scm^{-1} for the same LiTFSI concentration. However, PHU–N2N3-Ep showed a higher oxidation potential limitation of >4.24 V against >4.01 V versus Li/Li^+ for PHU–N2N3. Further, the long-term stability of those PHU-based SPEs with lithium metal has been confirmed from the exhaustive stripping and plating over 500+ cycles followed by post-mortem analysis, demonstrating constant overpotential. Finally, the potential of our PHUs as SPEs is demonstrated for Li|PHU–N2N3-Ep|LFP full solid-state batteries.

Experimental Section

2,2'-(ethylenedioxy)bis(ethylamine)(M_w~148.20) (EDEA), 4,7,10-trioxa-1,13-tridecanediamine (M_w~220.31) (TDD), poly(ethylene glycol) diglycidyl ether (M_w~500) (PEGDCE), anhydrous tetrahydrofuran (THF), lithium battery-grade, and lithium bis(trifluoromethanesulfonyl)imide (LiTFSI) were purchased from Sigma-Aldrich. Poly(ethylene glycol) bis(3-aminopropyl)- terminated (PEGTA)(Mw~1500) was bought from Acros organic chemical. Carbonated soybean oil (CSBO) was prepared following a previously published report.[42] Lithium metal foil (99.9%), lithium iron phosphate ($LiFePO_4$), poly(vinylidene fluoride), and Super-P were purchased from TOB chemicals. N-methyl-2-pyrrolidone (NMP) was bought from Alfa Aesar. Deuterated chloroform ($CDCl_3$) used for NMR spectroscopy was purchased from Eurisotop. All reactants and catalysts were used as received, without any further purification.

CHARACTERIZATION TECHNIQUES

Reproducibility of the results has been checked by performing at least three times any experiments. Results are reported as the average of those three trials. If a value was found to lie outside the admitted experimental error for a specific technique, it was discarded.

Rheology: Measurements were carried out on an Ares G2 rheometer from TA Instrument using parallel plates of 8 mm of diameter. Strain sweep experiment between 0.01 and 100% at a constant angular frequency of 10/s was used to assess the limit of the linear viscoelastic region (LVR) and to compare G' value. The frequency sweep test was carried out between 0.04 and 100 rad/s at a constant strain of 0.1% (in the LVR).

Fourier transform infrared spectra (FTIR) measurements: FTIR measurements were carried out on a Nicolet IS5 spectrometer (Thermo Fisher Scientific) equipped with a diamond attenuated transmission reflectance (ATR) device. 32 scans were recorded for each sample for different batches over the range of 4000–500 cm^{-1} with a normal resolution of 4 cm^{-1} and spectra were analysed with the ONIUM™ software.

Differential scanning calorimetry (DSC): DSC analysis was carried out on a Q1000 TA Instruments using standard aluminum pans, calibrated with indium, and nitrogen was used as a purge gas. The samples

Published in : ChemSusCheml (2025), vol. 18, e20500007
DOI: 10.1002/cssc.202500007
Status : Postprint (Author's version)

were analysed at a heating rate of 10°C min^{-1} over a temperature range from -80°C to 200°C under N_2 atmosphere and the analysis was repeated three times.

Thermogravimetric analysis (TGA): TGA was carried out using a Q500 from TA Instruments. Thermal degradation of samples was measured at a heating rate of 20°C min^{-1} over the temperature range of 0 to 600°C under a N_2 atmosphere.

X-ray photoelectron spectroscopy (XPS): XPS was performed using an SSI X-Probe (SSX 100/206) photoelectron spectrometer from Surface Science Instruments equipped with a monochromatized Al Kα (200 W) X-ray source. The batteries were disassembled and samples were mounted on an XPS sample holder in a glovebox prior to transferring to the XPS vacuum chamber in the flux of argon atmosphere. All binding energies were calculated according to the C-(C,H) component of the C1s peak fixed at 284.8 eV. Data analysis was carried out using the CasaXPS software. For the survey scan, a 1.0 eV step size was used and a 0.1 eV step size was utilized for high-resolution scans for all elements with 150 energy steps.

ELECTROCHEMICAL ANALYSIS

Electrochemical analysis of potentiostatic electrochemical impedance spectroscopy (PEIS), linear sweep voltammetry (LSV), chronoamperometry (CA), and galvanostatic cycling potential limitation (GCPL) were carried out on Biologic BCS-COM and VMP3 multichannel potentiostats using CR2032 coin cells. Reproducibility of the results has been checked by performing at least three times any electrochemical measurements. Results are reported as the average of those three trials. If a value was found to lie outside the admitted experimental error for a specific technique, it was discarded.

Potentiostatic electrochemical impedance spectroscopy (PEIS): Ionic conductivity of SPEs was determined by PEIS for symmetric stainless steel (SS j SEj SS) coin cells in the frequency range of 7 MHz–50 mHz, with applied single sinusoidal A.C. excitation voltage of 10 mV. The temperature dependence measurements were carried out from 20°C to 100°C by gradually increasing temperature at the rate of 0.33°Cmin[illegible]. 1 h was waited between each measurement to reach an equilibrium state. The experiments were repeated for several cells over different batches to avoid any errors.

Linear sweep voltammetry (LSV): Measurements were performed at various temperatures on asymmetric CR2032 coin cell as (Li|SPE|AI) over the potential range of 0–6.5 V (vs. Li/Li^+) at the scan rate of 0.5 mVs^{-1} at 60°C over few times.

Stripping and plating: The symmetric cell Li|SPE|Li was fabricated for stripping and plating analysis. The cells were charged and discharged for 1 h each for multiple cycles with the variable current densities and cut-off voltage of +4 V and -4 V at the room temperature under ambient atmosphere using BioLogic BCS-COM multichannel potentiostat.

Galvanostatic cycling potential limitation: Galvanostatic chargedischarge cycling and rate capabilities measurements for the LFP|SPE|Li cells were tested with a Biologic BCS-COM cycler for various batches of SPEs at different temperatures. The slurries for the cathodes were prepared from $LiFePO_4$, Super P, PVDF, and NMP via grinding using a mortar pestle and were further casted on carboncoated Al-foils

Published in : ChemSusCheml (2025), vol. 18, e20500007
DOI: 10.1002/cssc.202500007
Status : Postprint (Author's version)

using the doctor-blade technique. The coated slurries were then dried in an air oven for more than 6 h at 60°C prior to vacuum drying at 120°C for more than 24 h. The cathode components were maintained in the weight ratio of 7:2: 1 for LFP, Super P and PVDF. The cathodes and anodes were cut into disks of 14 mm diameter, and 16 mm in diameter for the electrolyte membranes.

SYNTHESIS

Synthesis of poly(hydroxyurethane) (PHU-NXNY): Bio-based cyclic carbonated soybean oil (CSBO) was synthesised by coupling of supercritical CO_2 with epoxidised soybean oil as reported elsewhere.[42] PHUs were obtained by reaction between CSBO and EDEA (N1), TDD (N2), and PEGTA (N3). The molar ratio of all (N1+N2+N3) combinations to CSBO was chosen to 3:1, corresponding to the assumption of all rings opening in CSBO.

As a typical example, for the synthesis of PHU–N2N3, 90 mg of CSBO (M_n~1250 g/mol), 81 mg of PEGTA (for 25 mol%, M_n~1500 g/ mol), and 35.69 mg of TDD (75 mol%, M_n~220.31 g/mol) were transferred in a small vial. These were dissolved in anhydrous THF via magnetic stirring at room temperature for >6 h. The resulting transparent solution was then drop cast on a Teflon mold followed by transfer to the vacuum oven. The temperature of the vacuum oven was set at 70°C for >12 h and later increased to 90°C for >24 h under dynamic vacuum. A similar procedure was followed for other PHU-NXNY and LiTFSI loaded PHU-NXNY (NX: N1, N2, N3) following the addition of salt solution to the initial mixture in case of the latter. After curing, the samples were transferred to the glove box.

Synthesis of poly(hydroxyurethane)-poly(epoxy) mixed networks (PHU—N2 N3-Ep): PEGTA and TDD in 25/75 molar ratio were mixed with CSBO to obtain PHU–N2N3 as mentioned above. For the mixed networks, PEGDCE was added to the reaction mixture required for PHU–N2N3 in 100 wt% with respect to CSBO. The most explored composition (PHU–N2N3-Ep) involved 70 mg of CSBO (MW~1250 g/mol), 63 mg of PEGTA (for 25 mol%, MW ~1500 g/mol), 27.75 mg of TDD (75 mol%, MW ~220.31 g/mol), and 70 mg of PEGDCE (MW ~500. 100 wt% relative to CBSO) dissolved in a small vial with the help of anhydrous THF by stirring for >6 h. The resulting transparent solution was then drop cast on a Teflon mold followed by transfer to the vacuum oven. The temperature of the vacuum oven was set at 70°C for >12 h and later increased to 90°C for >24 h under dynamic vacuum.

PREPARATION OF SOLID POLYMER ELECTROLYTES (SPES)

LiTFSI loading to the PHUs network was performed in the first step prior to thermal curing for electrolyte films. The dried films were transferred to the glove box and SPE films were peeled off from the Teflon molds and stored in the glove box before cell fabrication and characterization. The thickness of punched membranes was measured to be in the range of 100–200 µm. 2032-type coin cells were assembled using those free-standing SPE films sandwiched between SS|SS, SS|Li, Al/Al-C|Li, Li|Li, and Li|LFP electrode configurations to evaluate electrochemical performance.

Acknowledgements

AR and JFG are grateful to INNOVIRIS for supporting this research in the frame of the BRIDGE FUSE project (2019 - RPF – 8). C.D. is F.R.S.-FNRS Research Director and thanks F.R.S.-FNRS for financial support.

Conflict of Interests

The authors declare no conflict of interest.

Data Availability Statement

The data that support the findings of this study are available in the supplementary material of this article.

[1] X. Zeng, M. Li, D. Abd El-Hady, W. Alshitari, A. S. Al-Bogami, J. Lu, K. Amine, *Adv. Energy Mater.* **2019**, *9*, 1900161.

[2] N. Boaretto, I. Garbayo, S. Valiyaveettil-SobhanRaj, A. Quintela, C. Li, M. Casas-Cabanas, F. Aguesse, *J. Power Sources* **2021**, *502*, 229919.

[3] M. K. Hassan, N. Hameed, M. D. Hossain, M. R. Hasnat, G. Douglas, S. Pathirana, P. Rahnamayiezekavat, S. Saha, in *Fire, Vol. 6*, **2023**.

[4] J. Janek, W. G. Zeier, *Nat. Energy* **2023**, *8*, 230–240.

[5] J. Feng, L. Wang, Y. Chen, P. Wang, H. Zhang, X. He, *Nano Convergence* **2021**, *8*, 2.

[6] S. Zhao, Q. Wu, W. Ma, L. Yang, *Front. Chem.* **2020**, *8*.

[7] F. Ouhib, L. Meabe, A. Mahmoud, B. Grignard, J.-M. Thomassin, F. Boschini, H. Zhu, M. Forsyth, D. Mecerreyes, C. Detrembleur, *ACS Appl. Polym. Mater.* **2020**, *2*, 922–931.

[8] A. Raj, S. Panchireddy, B. Grignard, C. Detrembleur, J.-F. Gohy, *ChemSusChem* **2022**, *15*, e202200913.

[9] S. Zhou, S. Zhong, Y. Dong, Z. Liu, L. Dong, B. Yuan, H. Xie, Y. Liu, L. Qiao, J. Han, W. He, *Adv. Funct. Mater.* **2023**, *33*, 2214432.

[10] Y. Wu, Y. Li, Y. Wang, Q. Liu, Q. Chen, M. Chen, *J. Energy Chem.* **2022**, *64*, 62–84.

[11] P. Pal, A. Ghosh, *Solid State Ionics* **2018**, *319*, 117–124.

[12] S. Kurapati, S. S. Gunturi, K. J. Nadella, H. Erothu, *Polym. Bull.* **2019**, *76*, 5463–5481.

[13] Q. Wang, H. Zhang, Z. Cui, Q. Zhou, X. Shangguan, S. Tian, X. Zhou, G. Cui, *Energy Storage Mater.* **2019**, *23*, 466–490.

[14] Q. Zhang, K. Liu, F. Ding, X. Liu, *Nano Res.* **2017**, *10*, 4139–4174.

[15] M. S. M. Misenan, A. S. A. Khiar, T. Eren, *Polym. Int.* **2022**, *71*, 751–769.

[16] Z. Lv, Y. Tang, S. Dong, Q. Zhou, G. Cui, *Chem. Eng. J.* **2022**, *430*, 132659.

[17] A. Raj, B. Grignard, C. Detrembleur, J.-F. Gohy, *ECS Meeting Abstracts* **2022**, *MA2022-02*, 493.

[18] N. Yazie, D. Worku, N. Gabbiye, A. Alemayehu, Z. Getahun, M. Dagnew, *Materials for Renewable and Sustainable Energy* **2023**.

[19] M. Irfan, M. Atif, Z. Yang, W. Zhang, *J. Power Sources* **2021**, *486*, 229378.

[20] H. Wang, L. Sheng, G. Yasin, L. Wang, H. Xu, X. He, *Energy Storage Mater.* **2020**, *33*, 188–215.

[21] X. Zhao, C. Wang, H. Liu, Y. Liang, L.-Z. Fan, *Batteries & Supercaps* **2023**, *6*, e202200502.

[22] S. Kundu, Y. Ein-Eli, *J. Power Sources* **2023**, *553*, 232267.

[23] K. H. Park, Q. Bai, D. H. Kim, D. Y. Oh, Y. Zhu, Y. Mo, Y. S. Jung, *Adv. Energy Mater.* **2018**, *8*, 1800035.

[24] L. Bekaert, A. Raj, J.-F. Gohy, A. Hubin, F. De Proft, M. H. Mamme, *J. Phys. Chem. C* **2022**, *126*, 8227–8237.

[25] M. Balaish, J. C. Gonzalez-Rosillo, K. J. Kim, Y. Zhu, Z. D. Hood, J. L. M. Rupp, *Nat. Energy* **2021**, *6*, 227–239.

[26] O. Bayer, *Angew. Chem.* **1947**, *59*.

[27] M. Watanabe, S. Oohashi, K. Sanui, N. Ogata, T. Kobayashi, Z. Ohtaki, *Macromolecules* **1985**, *18*, 1945–1950.

[28] L. Porcarelli, K. Manojkumar, H. Sardon, O. Llorente, A. S. Shaplov, K. Vijayakrishna, C. Gerbaldi, D. Mecerreyes, *Electrochim. Acta* **2017**, *241*, 526–534.

[29] W. Zhu, B. Yang, X. Wang, L. Wang, X. Tang, C. Yang, *J. Appl. Polym. Sci.* **2002**, *83*, 103–111.

[30] S. R. Mustapa, M. M. Aung, M. Rayung, in *Polymers, Vol. 13*, **2021**.

[31] M. S. Su'ait, A. Ahmad, K. H. Badri, N. S. Mohamed, M. Y. A. Rahman, C. L. A. Ricardo, P. Scardi, *Int. J. Hydrogen Energy* **2014**, *39*, 3005–3017.

[32] R. Pathak, M. Kathalewar, K. Wazarkar, A. Sabnis, *Prog. Org. Coat.* **2015**, *89*, 160–169.

[33] L. Maisonneuve, O. Lamarzelle, E. Rix, E. Grau, H. Cramail, *Chem. Rev.* **2015**, *115*, 12407–12439.

[34] J. L. J. van Velthoven, L. Gootjes, D. S. van Es, B. A. J. Noordover, J. Meuldijk, *Eur. Polym. J.* **2015**, *70*, 125–135.

[35] L. Li, B. Zhao, G. Hang, Y. Gao, J. Hu, T. Zhang, S. Zheng, *Polymer* **2023**, *15*, 4634.

[36] F. Pei, L. Wu, Y. Zhang, Y. Liao, Q. Kang, Y. Han, H. Zhang, Y. Shen, H. Xu, Z. Li, Y. Huang, *Nat. Commun.* **2024**, *15*, 351.

[37] Y. He, C. Wang, R. Zhang, P. Zou, Z. Chen, S.-M. Bak, S. E. Trask, Y. Du, R. Lin, E. Hu, H. L. Xin, *Nat. Commun.* **2024**, *15*, 10015.

[38] S. D. Tillmann, P. Isken, A. Lex-Balducci, *J. Power Sources* **2014**, *271*, 239– 244.

Published in : ChemSusCheml (2025), vol. 18, e20500007
DOI: 10.1002/cssc.202500007
Status : Postprint (Author's version)

[39] A. Cornille, R. Auvergne, O. Figovsky, B. Boutevin, S. Caillol, *Eur. Polym. J.* **2017**, *87*, 535–552.

[40] N. K. Karan, D. K. Pradhan, R. Thomas, B. Natesan, R. S. Katiyar, *Solid State Ionics* **2008**, *179*, 689–696.

[41] i. J. R. M. M. A. Ratner, C. A. Vincent, Eds, in *Polymer Electrolyte Reviews 1*, Elsevier, Londen, **1987**.

[42] S. Panchireddy, B. Grignard, J.-M. Thomassin, C. Jerome, C. Detrembleur, *Polym. Chem.* **2018**, *9*, 2650–2659.